Characterization of Phosphatidylcholine Oxidation Products by MALDI MS^n

Whitney L. Stutts,[†] Robert F. Menger,[†] András Kiss,[‡] Ron M. A. Heeren,[‡] and Richard A. Yost*,[†]

[†]Department of Chemistry, University of Florida, Gainesville, Florida 32611-7200, United States

[‡]FOM Institute AMOLF, Science Park 104, 1098 XG Amsterdam, Netherlands

Supporting Information

ABSTRACT: Phospholipid oxidation has been implicated in the pathogenesis and progression of numerous age-related and neurodegenerative diseases. Despite these implications, this broad class of biomolecules remains poorly characterized. In this work, the fragmentation patterns of $[M + H]^+$ and $[M + Na]^+$ ions of intact phosphatidylcholine oxidation products (OxPCs) were characterized by matrix-assisted laser desorption/ionization tandem mass spectrometry (MALDI MS^n, $n = 2$, 3, and 4). MS^2 of both the $[M + H]^+$ and $[M + Na]^+$ ions of short-chain OxPCs yielded product ions related to the PC headgroup and the fatty acid substituents. MS^3 of the $[M + Na - N(CH_3)_3]^+$ ions yielded fragmentation indicative of the OxPC modification; specifically, a product ion corresponding to the neutral loss of CO_2 (NL of 44) was observed for OxPCs containing a terminal carboxylic acid rather than an aldehyde. Furthermore, MS^4 of the $[M + Na - HPO_4(CH_2)_2N(CH_3)_3]^+$ ions resulted in fragmentation pathways dependent on the *sn*-2 fatty acid chain length and type of functional group(s). Specifically, CHO-containing OxPCs with palmitic acid esterified to the *sn*-1 position of the glycerol backbone yielded a NL of 254, 2 u less than the nominal mass of palmitic acid, whereas the analogous terminal COOH-containing OxPCs demonstrated a NL of 256. Finally, the presence of a γ-ketone relative to the terminal carboxyl group resulted in C−C bond cleavages along the *sn*-2 substituent, providing diagnostic product ions for keto-containing OxPCs. This work illustrates the enhanced selectivity afforded by MS^n on the linear ion trap and develops a method for the identification of individual products of PC oxidation.

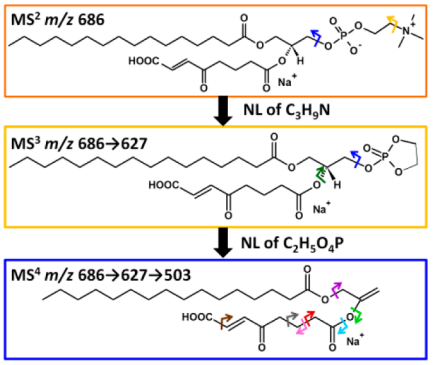

Lipid oxidation has been implicated in the pathogenesis or progression of various human disorders and diseases including Alzheimer's,[1−3] age-related macular degeneration,[4] atherosclerosis,[4,5] cataractogenesis,[4] multiple sclerosis,[6] and rheumatoid arthritis.[7] Probing lipid oxidation has proved challenging for a number of reasons, including the diversity of oxidation products, the instability of select oxidation products, and the sensitivity necessary to detect these oxidation products.[8] Furthermore, several studies have illustrated the various important biological activities of lipid oxidation products and have shown that many of these activities (e.g., inflammatory vs anti-inflammatory) are dependent on the specific chemical structure of the oxidized species;[9] the type of modification to the *sn*-2 substituent (terminal carboxylic acid vs terminal aldehyde), the chemical bond linking the *sn*-1 substituent (ether vs ester), the fatty acid chain length, and the charge on the headgroup have all been shown to affect the biological activities of lipid oxidation products.[9−13] Certain lipids known to be susceptible to oxidation have also been reported to be enriched in specific cells and tissues; one example is plasmalogens, a type of phospholipid containing a vinyl ether moiety at the *sn*-1 position, which are abundant in cardiac and nervous tissue.[14] Thus, there is growing interest in developing methods for characterizing and identifying lipid oxidation products in biological samples.[15]

Biochemical assays, such as the thiobarbituric acid (TBA) assay,[16] have been widely used to detect total lipid oxidation; however, these assays lack the selectivity needed for structural elucidation.[17] Diene conjugation, measured by UV absorbance at 234 nm, has also been utilized to determine the extent of lipid oxidation, but this method also suffers from poor selectivity.[17] Mass spectrometry (MS) has become increasingly utilized in lipid oxidation research due to the ability to characterize biomolecules based on their mass-to-charge (m/z) ratios, yielding superior selectivity relative to the aforementioned techniques.[18−20] Despite the various challenges, several MS methods have been developed for the analysis of the oxidatively modified phospholipids (OxPLs). Gas chromatography−mass spectrometry (GC-MS) and liquid chromatography−mass spectrometry (LC-MS) have been used for identification and quantitation of phospholipid oxidation products;[21−26] however, many of these methods require hydrolysis of the oxidized free fatty acid moieties from the phospholipid headgroup and extensive derivatization prior to analysis.

More recently, soft ionization methods have been employed for the analysis of OxPLs without derivatization.[27−37] Electrospray ionization mass spectrometry (ESI MS) combined with reversed-phase high-performance liquid chromatography (RP-HPLC) has become the most widely used method for the analysis of OxPLs.[19] This method offers several advantages. First, OxPLs readily ionize by ESI and RP-HPLC offers chromatographic separation based on fatty acid composition. Second, these methods are amenable to tandem mass spectrometry (MS^n), though in most cases only two stages of MS (i.e., MS^2) have been performed.[18,19] Matrix-assisted laser desorption/ionization (MALDI) has also been used to investigate OxPLs,[38] but few published studies have used this ionization method in spite of the many inherent advantages.[39] In comparison to LC coupled with ESI MS, MALDI MS requires less sample and offers more rapid analysis. Furthermore, MALDI is less sensitive to salts and other impurities found in complex biological samples;[17] in fact, addition of salts is often advantageous for the structural elucidation of various phospholipids by MALDI MS^n.[35,40−42] Additionally, MALDI can be coupled with mass spectrometric imaging (MSI) techniques for in situ detection and localization of phospholipids in biological tissues.[41−44]

This investigation characterized oxidation products of phosphatidylcholines, the most abundant phospholipids in cell membranes, by MALDI MS^n using a linear ion trap (LIT) mass analyzer. The MS^n (where n = 2, 3, or 4) capabilities of the LIT were exploited for enhanced selectivity, resulting in more reliable characterization of the collision-induced dissociation (CID) fragmentation pathways of OxPCs. Additionally, preliminary results illustrate the utility of the developed MALDI MS^n method for identifying and imaging these OxPCs in biological tissues.

EXPERIMENTAL SECTION

Chemicals. Avanti Polar Lipids (Alabaster, AL) was the source for all lipid standards except 1-palmitoyl-2-(5-keto-6-octene-dioyl)-*sn*-glycero-3-phosphatidylcholine (KOdiAPC), which was purchased from Cayman Chemical (Ann Arbor, MI). MALDI matrix, 2,5-dihydroxybenzoic acid (DHB), was purchased from Acros Organics (Geel, Belgium). Sodium acetate trihydrate (NaOAc) and HPLC-grade water and methanol were purchased from Fisher Scientific (Fair Lawn, NJ). Ethanol (200 proof) was purchased from Decon Laboratories (King of Prussia, PA).

Sample Preparation. The short-chain oxidation product (OxPC) standards listed in Table 1 were dissolved in cold, degassed ethanol to a concentration of 100 ppm (100 ng in 1 μL). A MALDI matrix solution consisting of 40 mg/mL DHB in 70:30 methanol:water (v/v) and 10 mM NaOAc (final concentration) was prepared. Sodium acetate was added to enhance the relative intensity of the $[M + Na]^+$ ions, which yielded more structurally informative fragmentation. OxPC standards were deposited atop a 384-well stainless steel MALDI plate using a modified dried-droplet method.[45] For this method, 1 μL of the 100 ppm OxPC standards followed by 1 μL of MALDI matrix were pipetted into the sample wells. The solvent was allowed to evaporate in ambient air, resulting in matrix−analyte cocrystals. The lowest concentration of standards evaluated was 10 ppm (10 ng in 1 μL), and at this concentration analytes were still observed above baseline; however, ion intensities were insufficient for some multistage experiments.

Table 1. Nomenclature of the OxPC Standards Analyzed[a]

chemical name [shorthand]	R_1	R_2'	monoisotopic mass
1-palmitoyl-2-(5-oxo-valeroyl)-*sn*-glycero-3-phosphocholine [POVPC]	16:0	5:0 (CHO)	593.37
1-palmitoyl-2-glutaryl-*sn*-glycero-3-phosphocholine [PGPC]	16:0	5:0 (COOH)	609.36
1-palmitoyl-2-(9-oxo-nonanoyl)-*sn*-glycero-3-phosphocholine [PONPC]	16:0	9:0 (CHO)	649.43
1-palmitoyl-2-azelaoyl-*sn*-glycero-3-phosphocholine [PAzPC]	16:0	9:0 (COOH)	665.43
1-palmitoyl-2-(5-keto-6-octene-dioyl)-*sn*-glycero-3-phosphocholine [KOdiAPC]	16:0	8:1 (COOH)[b]	663.37

[a]Nomenclature according to the LIPID MAPS systematic naming is used (www.lipidmaps.org). R_1 represents the number of carbons and double bonds (C:DB) in the fatty acid substituents esterified to the *sn*-1 position of the glycerol backbone. R_2' represents the number of carbons and double bonds in the oxidatively truncated fatty acid substituent. These *sn*-2 acyl groups contain 5−9 carbon atoms and a terminal aldehyde (CHO) or carboxyl group (COOH). [b]In addition to the terminal α,β-unsaturated carboxyl group, the *sn*-2 tail of KOdiAPC also contains a ketone at C_5.

To illustrate the potential for identification and MSI of OxPCs, spinal cord tissue from the lumbar region of adult, female Sprague−Dawley rats (Harlan, San Diego, CA) was utilized. Animal studies, approved by the local IACUC, were carried out by Nigel Calcutt at the University of California, San Diego and were performed in an AAALAC-approved vivarium. Following euthanasia, excised tissue was immediately flash-frozen in liquid nitrogen and stored at −80 °C until further use. Tissue was sectioned at −25 °C using a Microm HM 505E cryostat (Walldorf, Germany). To avoid analyte ion suppression resulting from tissue mounting media (e.g., optimal cutting temperature polymer),[46] spinal cord tissue was fused to the cutting stage using HPLC-grade water. Cross sections (10 μm thick) were thaw-mounted atop cold glass microscope slides and subsequently dried in a vacuum desiccator for approximately 30 min to remove excess water. The slides were then spray coated with MALDI matrix using a glass Type A Meinhard nebulizer (Golden, CO) and nitrogen (30 PSI) as the nebulizing gas. Matrix was applied until a homogeneous layer of matrix−analyte cocrystals was observed over the entire tissue.

Mass Spectrometry. Mass spectra were acquired in positive ion mode using an intermediate-pressure (75 mTorr) MALDI-LIT mass spectrometer, a Thermo Scientific MALDI LTQ XL (San Jose, CA). This instrument was equipped with a 337 nm nitrogen laser with a 60 Hz repetition rate and 100 μm laser spot diameter. Laser energies of 2.0−8.0 μJ per laser shot and 3−4 laser shots per raster spot were used in these experiments; automatic gain control (AGC) was toggled off. Each mass spectrum presented represents an average of 100 analytical scans, unless otherwise noted. For MSI experiments, images were generated using Thermo ImageQuest 1.0.1 software (San Jose, Ca). Mass spectral images generated following one stage of mass analysis (MS) were normalized to the total ion current (TIC). For images generated from higher stages of mass analysis, the intensity of the most abundant product ion was plotted at each pixel and was not normalized to

Table 2. Product Ions Observed in the MS^2 Spectra of $[M + H]^+$ Ions of PAzPC, PONPC, PGPC, POVPC, and KOdiAPC[a]

neutral loss composition	PAzPC *m/z* 666	PONPC *m/z* 650	PGPC *m/z* 610	POVPC *m/z* 594	KOdiAPC *m/z* 664
$[H_2PO_4(CH_2)_2N(CH_3)_3]^{+b}$	184 (100)	184 (100)	184 (100)	184 (100)	184 (100)
$-R_1{=}C{=}O$	428 (0.4)	412 (1.6)	372 (0.6)	356 (0.5)	426 (1.0)
$-R_2'{=}C{=}O$	**496 (1.1)**	**496 (3.4)**	**496 (1.1)**	**496 (0.7)**	**496 (2.5)**
$-R_1COOH$	**410 (1.2)**	**394 (3.5)**	**354 (1.2)**	**338 (0.8)**	**408 (1.4)**
$-R_2'COOH$	478 (0.5)	478 (2.1)	478 (0.7)	478 (0.7)	478 (1.1)
$-HPO_4(CH_2)_2N(CH_3)_3$	483 (0.3)	467 (1.2)	427 (0.3)	411 (0.5)	481 (1.2)
$-H_2O$	648 (1.5)	NA	592 (1.1)	NA	646 (9.6)
$-N(CH_3)_3$	NA	591 (0.4)	NA	NA	605 (8.9)
$-CO_2$	NA	NA	566 (0.1)	NA	620 (1.9)

[a]Relative abundances (%) for each product ion are given in parentheses. The abundance was rounded to the nearest tenth of a percent. NA = relative abundances ≤ 0.1%. Most abundant loss of *sn*-1 and *sn*-2 are indicated in bold type. [b]Indicates a product ion rather than a NL.

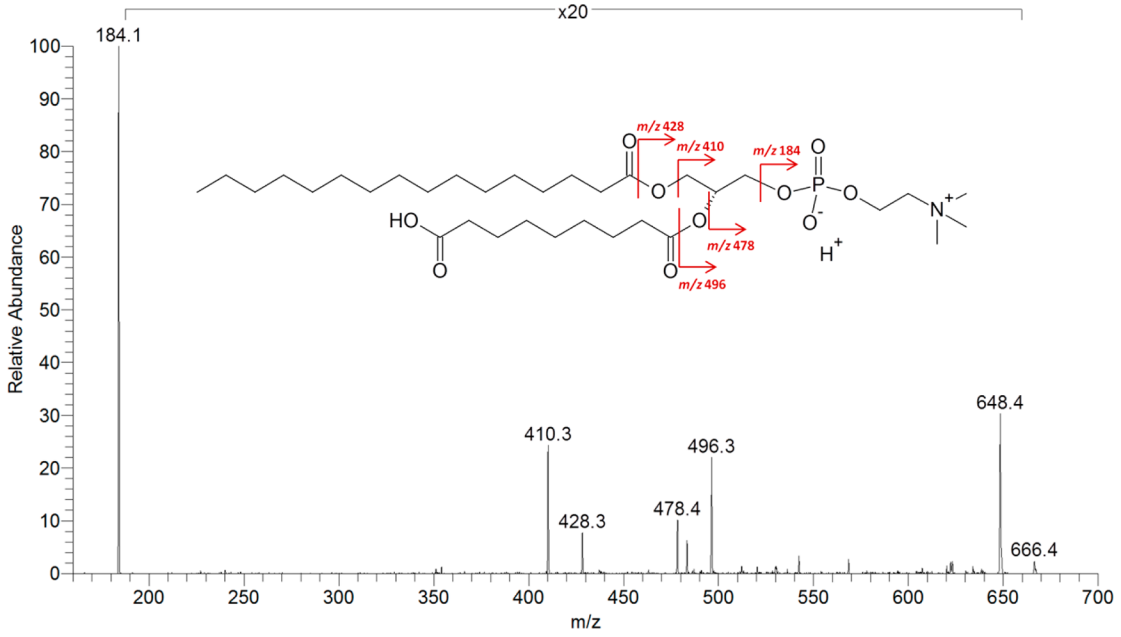

Figure 1. MS^2 product ion spectrum of *m/z* 666, the $[M + H]^+$ ion of PAzPC. The structure and proposed fragmentation of the ion at *m/z* 666 are also shown.

TIC. All other data processing was performed using Thermo QualBrowser 2.0.7 (San Jose, Ca).

For MS^2 experiments, a precursor ion isolation width of 1.2 u was utilized. For MS^3, the precursor ion isolation widths for the first and second isolation events were adjusted to 1.5 and 2.0 u, respectively. Lastly, for MS^4, isolation widths of 1.5, 2.0, and 2.5 u were utilized for the first, second, and third isolation events, respectively. By widening these isolation windows for MS^3 and MS^4, precursor ion isolation efficiencies were enhanced. Therefore, signal loss was minimized when going from MS^2 to MS^3. However, MS^4 typically resulted in a signal loss of approximately an order of magnitude compared to MS^3.

MS^2, MS^3, and MS^4 experiments were performed using CID. Collision energies were optimized to achieve maximum product ion intensity. In general, the precursor ion was depleted to <20% of the most intense fragment ion; however, without exception, the precursor ion was detected above the baseline. For precursor ions with higher *m/z* values (greater than *m/z* 599), the *q* of activation (q_{act}) was reduced to 0.22 (typically q_{act} = 0.25 on the LTQ XL), when necessary, to decrease the low-mass cutoff (LMCO). Specifically, the LMCO was decreased to observe the product ion at *m/z* 184 for protonated OxPCs.

To validate several proposed fragmentation pathways and product ion identifications, accurate mass measurements were performed using a 7T hybrid LIT-Fourier transform ion cyclotron resonance (FTICR) mass spectrometer, the Finnigan LTQ FT (Thermo Fisher Scientific, Bremen, Germany). This instrument was equipped with a Thermo Scientific nanospray ionization (NSI) source. For these experiments, OxPC standards, diluted to 1000 nM in ethanol, were directly infused at a flow rate of 0.5 μL/min, and the NSI spray voltage was set to +2 kV. The heated capillary on the LTQ was held at +39 V and 200 °C. MS^n isolation and excitation were performed in the LIT, whereas mass analysis of the product ions was conducted in the ICR cell. AGC was toggled on for all experiments with a maximum injection time of 100 ms. For MS^n experiments on the LTQ FT, the parameters for precursor ion isolation widths were the same as those outlined above, with the exception of the third isolation event in MS^4, which was lowered from 2.5 to 2.0 u. Additionally, collision energies were optimized as described above. The FT portion of the instrument was operated in wide scan mode at a resolving power of 100 000 with 50 analytical scans (each composed of 10 microscans) averaged to obtain accurate mass values.

Table 3. Product Ions Observed in MS^2 Spectra of $[M + Na]^+$ Ions of PAzPC, PONPC, PGPC, POVPC, and KOdiAPC[a]

neutral loss composition	PAzPC m/z 688	PONPC m/z 672	PGPC m/z 632	POVPC m/z 616	KOdiAPC m/z 686
$-N(CH_3)_3$	629 (100)	613 (100)	573 (100)	557 (100)	627 (100)
$-HPO_4(CH_2)_2N(CH_3)_3$	505 (12.2)	489 (7.5)	449 (15.1)	433 (10.5)	503 (7.2)
$-R_2'COONa$	478 (0.3)	478 (0.1)	478 (0.2)	478 (0.3)	478 (0.2)
$-R_1COOH$	432 (0.2)	416 (0.1)	376 (0.1)	360 (0.1)	430 (0.1)
$-R_2'COOH$	500 (0.1)	500 (0.1)	500 (0.3)	500 (0.2)	500 (0.2)
$-R_1COOH$ and $N(CH_3)_3$	373 (0.1)	357 (0.1)	317 (0.1)	301 (0.1)	371 (0.1)
$-R_2'COOH$ and $N(CH_3)_3$	441 (0.1)	NA	441 (0.4)	441 (0.3)	441 (0.2)
$-R_2'{=}C{=}O$	NA	NA	518 (0.6)	NA	518 (0.1)

[a]Relative abundances (%) for each product ion are given in parentheses. The abundance was rounded to the nearest tenth of a percent. NA = relative abundances ≤0.05%.

RESULTS AND DISCUSSION

Ionization of unmodified PCs by MALDI produces both protonated species, $[M + H]^+$, and alkali metal adducts such as $[M + Na]^+$.[18] Depending on the precursor ion selected, the fragmentation pathways observed by MS^2 vary greatly.[47] In contrast to the $[M + H]^+$ ions of unmodified PCs, which yield one predominant MS^2 product ion (m/z 184) and little structural information, CID of the $[M + Na]^+$ ions yields many structurally informative product ions.[40,48] In this work, MALDI MS utilizing DHB as a positive-mode matrix produced both protonated and sodiated ions of OxPCs. Subsequently, the fragmentation pathways of the $[M + H]^+$ and $[M + Na]^+$ ions were explored for each of the OxPCs listed in Table 1.

MS^2 Characterization of the $[M + H]^+$ Ions of Short-Chain OxPCs. The observed MS^2 product ions resulting from CID of the $[M + H]^+$ ions of PAzPC, PONPC, PGPC, POVPC, and KOdiAPC are listed in Table 2. Many of these product ions are in accordance with the ESI MS^2 fragmentation of $[M + H]^+$ ions of 1-palmitoyl-2-linoleoyl-*sn*-glycero-3-phosphocholine (PLPC) and 1-palmitoyl-2-arachidonoyl-*sn*-glycero-3-phosphocholine (PAPC) oxidation products reported by Reis et al.[33] Similar to unmodified PCs, following CID of the $[M + H]^+$ ion, short-chain OxPCs yielded a dominant product ion at m/z 184, corresponding to the protonated phosphocholine headgroup ($[H_2PO4(CH_2)_2N(CH_3)_3]^+$).[49,50] Although much lower in abundance (0.5−4% relative abundance), the product ions corresponding to the neutral losses (NLs) of the fatty acid moieties, as free acids or as ketenes, were also observed. These product ions were reported previously in ESI MS^2 studies of unmodified PCs and allowed for differentiation of positional isomers based on the relative abundances of the *sn*-1 and *sn*-2 ketene losses; the product ion corresponding to the *sn*-2 ketene NL ($-R_2{=}C{=}O$) demonstrated greater abundance than the product ion due to the *sn*-1 ketene NL ($-R_1{=}C{=}O$).[50] This trend was also observed for all short-chain OxPCs studied in this work; that is, the loss of the saturated *sn*-1 ketene was, in all cases, less abundant than the loss of the oxidized *sn*-2 ketene. Furthermore, the modified *sn*-2 fatty acid chain was preferentially lost as the ketene ($-R_2'{=}C{=}O$) while the *sn*-1 fatty acid chain was preferentially lost as the free acid ($-R_1COOH$).

As a specific example, Figure 1 illustrates these fragmentation pathways for MS^2 of the $[M + H]^+$ ion of PAzPC (m/z 666). The product ion corresponding to the phosphocholine headgroup, m/z 184, was the base peak; all other product ions were observed below 2% relative abundance. Upon 20× magnification of the upper mass region of the spectrum (greater than m/z 200), product ions related to the fatty acid tails were observed. The losses of the *sn*-2 tail as the ketene (NL of 170) and as the free acid (NL of 188), although lower in abundance, were observed at m/z 496 and 478, respectively. Likewise, losses of the *sn*-1 tail as the ketene and as the free acid were observed at m/z 428 and 410, respectively; however, the *sn*-1 tail was preferentially lost as the free acid instead of the ketene. The MS^2 product ion spectrum of m/z 666 also illustrates that the ion corresponding to the *sn*-2 ketene loss (m/z 496) was greater in abundance than that of the *sn*-1 ketene loss (m/z 428).

Although structural information may be obtained from CID of the $[M + H]^+$ ions, the majority of the product ion intensity falls at m/z 184, a structurally uninformative fragment ion with regards to the substituents bound to the *sn*-1 and *sn*-2 positions of the glycerol backbone. Thus, fragmentation of the $[M + H]^+$ ion presents a relatively inefficient method for determining fatty acid composition and position. Accordingly, the fragmentation pathways related to the $[M + Na]^+$ ions of OxPCs were explored.

MS^n Characterization of the $[M + Na]^+$ Ions of Short-Chain OxPCs. The MS^n product ion spectra of the short-chain products studied illustrated distinct fragmentation patterns for the $[M + Na]^+$ ions. For each of the OxPCs, the MS^2 product ions resulting from CID of the $[M + Na]^+$ precursor ions are listed in Table 3. Many of these product ions are in agreement with ESI MS^2 product ions previously observed following CID of PLPC and PAPC oxidation products.[33] Characteristic MS^2 fragmentation resulting in product ions produced from NLs of 59 (trimethylamine) and 183 (phosphocholine) were observed.[33,47,51] Although these were the two most abundant product ions of each of the short-chain OxPCs investigated in this work, product ions resulting from the NLs of the *sn*-1 and *sn*-2 fatty acid tails were also observed following CID.

In MS^2, the *sn*-1 tail was lost as the free acid or as the concurrent loss of the *sn*-1 free fatty acid and trimethylamine. Additionally, various losses of the *sn*-2 tail were observed for each of the OxPCs investigated. For all of the short-chain OxPCs except PGPC, the *sn*-2 tail was preferentially lost as the neutral, sodiated free acid; PGPC fragmentation also yielded a loss of the *sn*-2 tail as the neutral, sodiated free acid, but the *sn*-2 ketene loss (NL of 114) was more abundant.

Product ions resulting from the concurrent loss of the *sn*-2 tail and the trimethylamine were also observed at approximately equal or greater relative abundance than that of the product ions resulting from concurrent loss of the *sn*-1 tail and the trimethylamine. This fragmentation pathway has been previously reported for lithium adducts of unmodified PCs.[50] However, the opposite trend was previously observed (i.e., the $[M + Li - R_1COOH - N(CH_3)_3]^+$ ion was greater in abundance than the $[M + Li - R_2COOH - N(CH_3)_3]^+$ ion).[50]

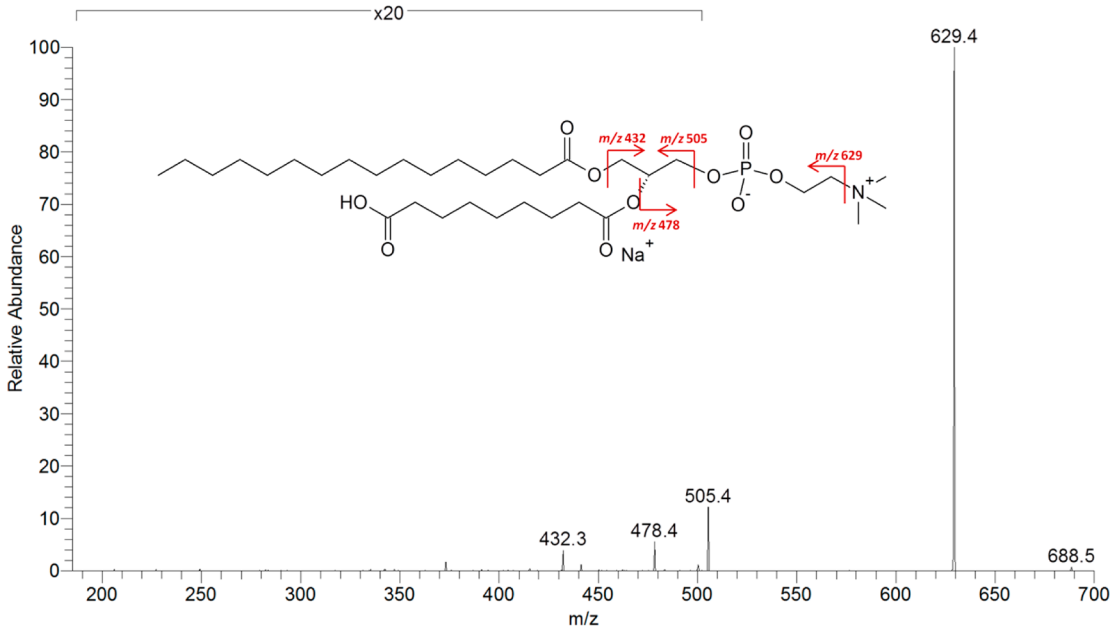

Figure 2. MS^2 product ion spectrum of m/z 688, the $[M + Na]^+$ ion of PAzPC. The structure and proposed fragmentation of the ion at m/z 688 are also shown.

Table 4. Product Ions Observed in MS^3 Spectra of $[M + Na - N(CH_3)_3]^+$ Ions of PAzPC, PONPC, PGPC, POVPC, and KOdiAPC[a]

neutral loss composition	PAzPC m/z 629	PONPC m/z 613	PGPC m/z 573	POVPC m/z 557	KOdiAPC m/z 627
$-HPO_4(CH_2)_2$	505 (100)	489 (100)	449 (100)	433 (100)	503 (100)
$-HPO_4(CH_2)_2$ and Na	483 (0.3)	467 (0.4)	427 (0.4)	411 (1)	481 (0.5)
$-R_2'COOH$	441 (0.5)	441 (0.7)	441 (2.5)	441 (2.5)	441 (2.6)
$-R_2'COOH$ and C_2H_2	415 (0.1)	415 (0.1)	415 (0.1)	415 (0.2)	415 (0.2)
$-R_1COOH$	373 (0.4)	357 (0.5)	317 (0.5)	301 (0.5)	371 (0.4)
$-R_1COOH$ and $HPO_4(CH_2)_2$	249 (0.8)	NA	NA	NA	NA
$-R_1COOH$, $HPO_4(CH_2)_2$, and Na	227 (0.3)	NA	NA	NA	NA
$-CO_2$	585 (0.1)	NA	529 (0.1)	NA	583 (0.1)
$-C_6H_6O_3$ and $HPO_4(CH_2)_2$[b]	NA	NA	NA	NA	377 (1.1)

[a]Relative abundances (%) for each product ion are given in parentheses. The abundance was rounded to the nearest tenth of a percent. NA = relative abundances $\leq$ 0.05%. [b]Fragmentation resulting from proposed intramolecular retro-ene reaction discussed later in the text.

Therefore, the oxidative modification to the *sn*-2 tail or the sodium likely influences this fragmentation pathway.

Figure 2 illustrates the MS^2 fragmentation pathways of the PAzPC $[M + Na]^+$ ion (m/z 688). CID of m/z 688 resulted in a predominant product ion at m/z 629, resulting from the NL of trimethylamine (NL of 59). Additionally, NLs of the phosphocholine headgroup (NL of 183), sodiated *sn*-2 free fatty acid (NL of 210), and *sn*-1 free fatty acid (NL of 256) were observed at m/z 505, 478, and 432, respectively. At even lower relative abundances (<0.1%), but still detectable above baseline, product ions corresponding to the loss of the *sn*-2 free acid (m/z 500), *sn*-1 free acid combined with trimethylamine (m/z 373), and *sn*-2 free acid combined with trimethylamine (m/z 441) were observed.

Although MS^2 provides useful structural information, in situ identification of these OxPCs would likely be confounded by isobaric species. Thus, further stages of MS were utilized for enhanced selectivity and increased structural information. For these studies, MS^3 was performed on the product ions resulting from the loss of trimethylamine (NL of 59). Table 4 summarizes the product ions and relative abundances observed in the MS^3 spectra from the $[M + Na - N(CH_3)_3]^+$ ions of the short-chain OxPCs. As was shown previously for unmodified PCs,[47] the predominant MS^3 product ion observed resulted from the loss of the remaining portion of the phosphocholine headgroup (cyclophosphane; NL of 124). Although much lower in abundance, MS^3 of these OxPCs yielded product ions corresponding to the NLs of the *sn*-1 and *sn*-2 tails (both as the free acid). In contrast to MS^2 fragmentation, the sodium was not lost with the *sn*-2 tail. Instead, a minor product ion corresponding to the NL of cyclophosphane with sodium (NL of 146) was present in the MS^3 spectra from each of the oxidation products studied. Furthermore, an MS^3 product ion at m/z 415, proposed to be the loss of the *sn*-2 tail combined with the loss of acetylene (possibly from the remaining portion of the PC headgroup), was observed in the MS^3 spectra from each of the short-chain OxPCs. Unfortunately, this ion was generally not detected in the high resolution experiments, most likely because of the low abundance of this ion in MS^3 spectra. However, in one experiment with PAzPC this product ion was detected above the noise with a mass error of 4.23 ppm. Lastly, structurally informative product ions, which were only observed for OxPCs containing a terminal carboxylic acid on the *sn*-2 fatty acid tail, resulted from the loss of CO_2 (NL of 44). Thus,

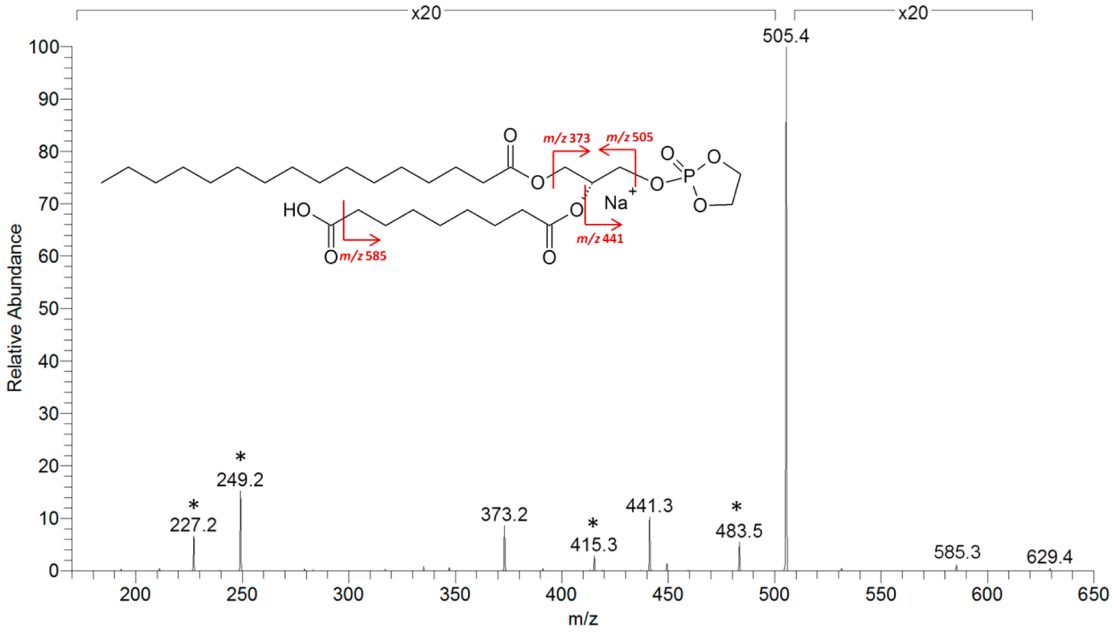

Figure 3. MS^3 product ion spectrum of m/z 688→629, the $[M + Na - N(CH_3)_3]^+$ ion of PAzPC. The structure and proposed fragmentation of the ion at m/z 629 are also shown. Fragmentation pathways leading to the product ions marked with an asterisk are discussed in the text.

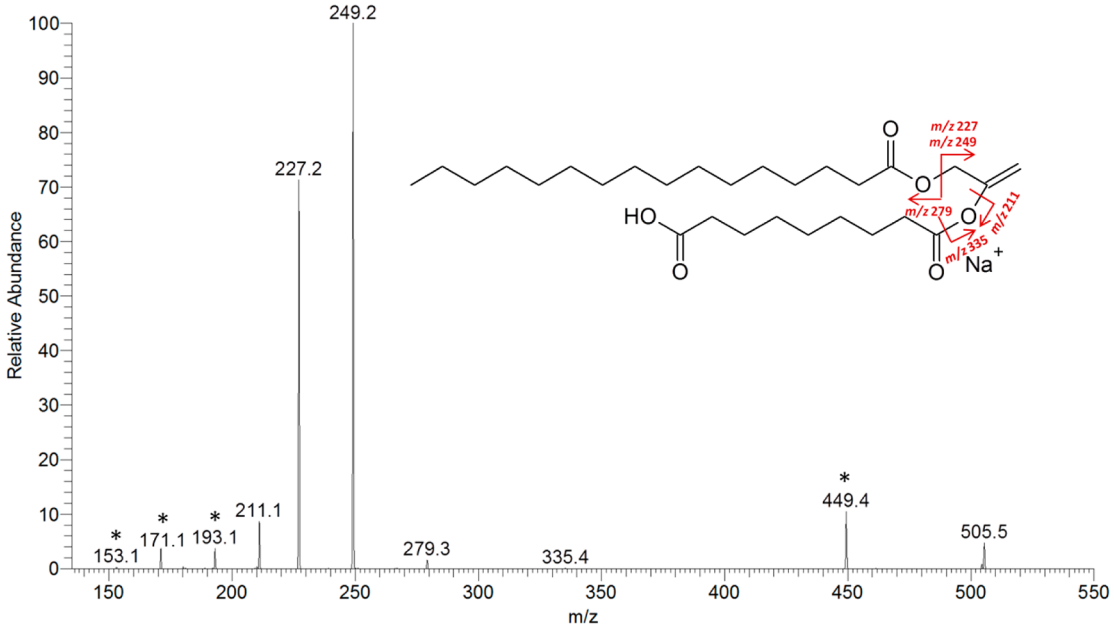

Figure 4. MS^4 product ion spectrum of m/z 688→629→505, the $[M + Na - HPO_4(CH_2)_2N(CH_3)_3]^+$ ion of PAzPC. The proposed structure and fragmentation of the ion at m/z 505 are also shown. Product ions marked with an asterisk are discussed in the text.

the NL of CO_2 results in a diagnostic product ion that can be used to differentiate short-chain OxPCs containing a terminal carboxyl group from those containing a terminal aldehyde.

Figure 3 illustrates the MS^3 product ion spectrum and fragmentation pathways of the $[M + Na - N(CH_3)_3]^+$ ion (m/z 629) of PAzPC. In addition to the product ions observed for all OxPCs investigated, MS^3 product ions of PAzPC resulting from the concurrent loss of the *sn*-1 free acid and cyclophosphane or the sodiated cyclophosphane were observed at m/z 249 and 227, respectively. Interestingly, this MS^3 fragmentation pathway was not observed for any of the other short-chain products studied in this work. Furthermore, since PAzPC contains a terminal carboxylic acid group on the *sn*-2 tail, a loss of CO_2 (NL of 44) was observed, indicating cleavage of the α-bond relative to the terminal functional group.

MS^4 fragmentation of the $[M + Na - HPO_4(CH_2)_2N(CH_3)_3]^+$ ions varied drastically depending on the *sn*-2 fatty acid length and composition. Despite the variation, the observed product ions yield valuable structural information. Figure 4 illustrates the characteristic fragmentation observed in the MS^4 product ion spectrum of m/z 688→629→505 corresponding to the $[M + Na - HPO_4(CH_2)_2N(CH_3)_3]^+$ ion of PAzPC. Although recent evidence has suggested that either a 5- or 6-member cyclic structure forms for unmodified PCs prior to MS^4,[50] at present, the exact structure of this ion is unclear due to the presence of the modified *sn*-2 fatty acid. For

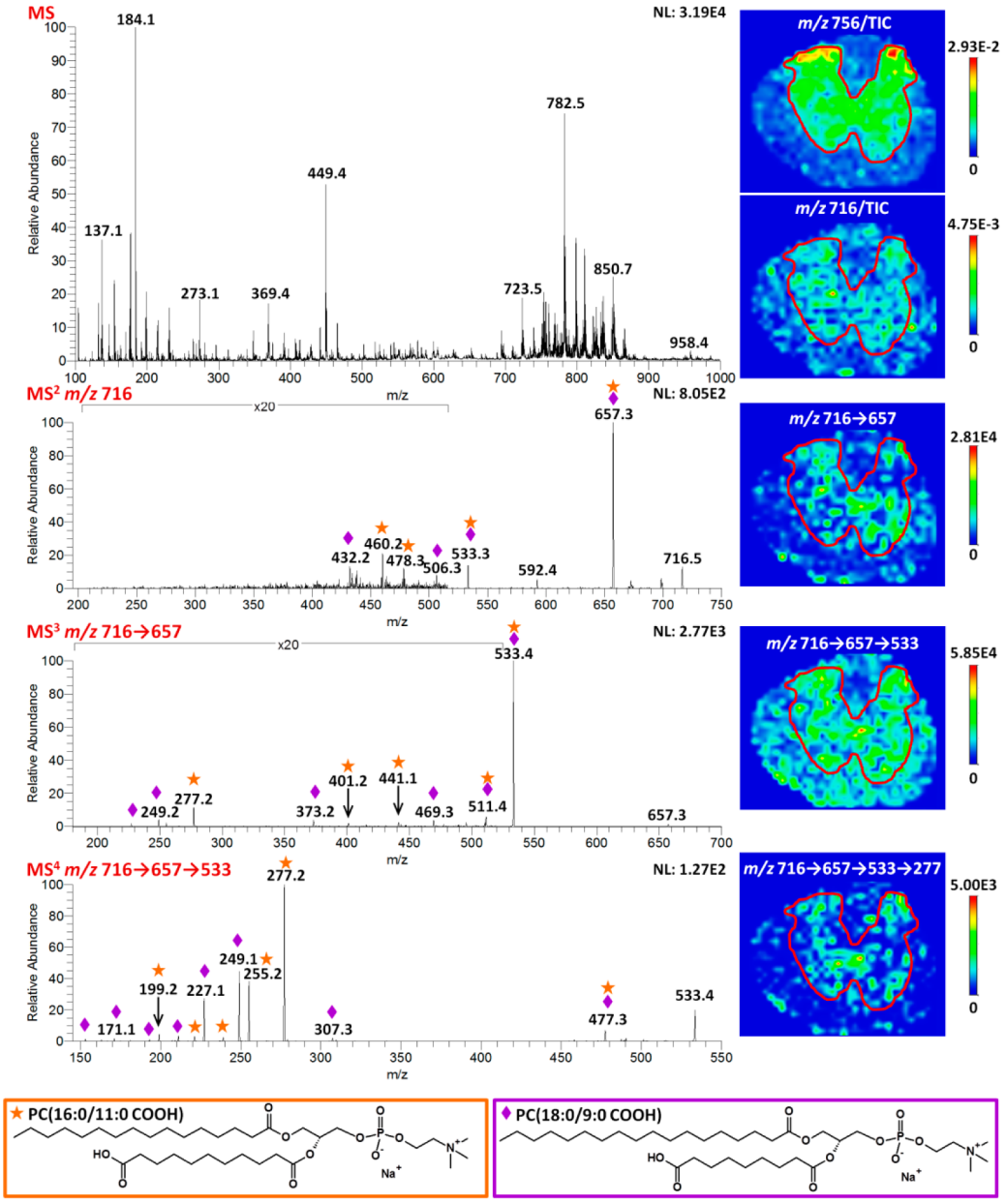

Figure 5. Identification and imaging of two proposed OxPCs at m/z 716. The MS spectrum illustrates the complex mixture of biomolecules observed in tissue. MS^2, MS^3, and MS^4 spectra and images demonstrate the feasibility of identifying and localizing OxPCs in biological tissues using the MALDI MS^n methods developed in this work. On the basis of the product ions observed, two isomeric OxPCs were identified, PC(16:0/11:0 COOH) and PC(18:0/9:0 COOH). The proposed structures are displayed in the orange and purple boxes and the product ions specific to each of these OxPCs are indicated by orange stars and purple diamonds for PC(16:0/11:0 COOH) and PC(18:0/9:0 COOH), respectively. Furthermore, upon comparison of the MS^n images of m/z 716 ($[PC(16:0/11:0\ COOH) + Na]^+$ and $[PC(18:0/9:0\ COOH) + Na]^+$) to the MS image of m/z 756 ($[PC(16:0/16:0) + Na]^+$, a PL known to localize in the gray matter of rat spinal cord), the ions related to the OxPCs appear mostly in the gray matter (outlined in red).

simplicity, this ion is displayed without the ring structure. Regardless of the structure, the predominant product ions at m/z 249 and 227 resulted from the NL of the *sn*-1 fatty acid tail and the *sn*-1 tail with sodium, respectively. These product ions, in addition to the product ions at m/z 279, 211, 193, 171, and 153, which were attributed to $[R_1COOH + Na]^+$, $[R_2'COOH + Na]^+$, $[R_2'COOH + Na - H_2O]^+$, $[R_2'COOH + H - H_2O]^+$, and $[R_2'COOH + H - 2H_2O]^+$, respectively, confirmed the identification of both fatty acid substituents of PAzPC. Furthermore, the NL of 56 (m/z 449) was observed in the MS^4 product ion spectrum of PAzPC and likely corresponds to the loss of C_3H_4O as previously reported for MS^n on the $[M + Na]^+$ ions of triacylglycerols.[52] However, this loss of 56 was observed in the MS^4 product ion spectrum from each of the OxPCs investigated in this work and is therefore less structurally informative than the product ions related to the fatty acid tails.

The MS^4 product ion spectra from CID of the $[M + Na - HPO_4(CH_2)_2N(CH_3)_3]^+$ ion of the other OxPCs listed in Table 1 are included in the Supporting Information (Figures S-1−S-4). Many product ions analogous to those described above for PAzPC were also observed in the MS^4 spectra of the other OxPCs; however, MS^4 product ions specific to the type of oxidative modification were also detected. One diagnostic

fragmentation pathway was the loss of the *sn*-1 fatty acid tail; in contrast to the carboxylic acid derivatives, the OxPCs containing a terminal aldehyde lost the *sn*-1 tail (palmitic acid; 256 u) as the NL of 254 rather than 256. Based on previously reported MS^2 fragmentation of $[M + Li]^+$ ions of unmodified PCs[53] and triacylglycerols,[52] the NL of 254 likely results from the elimination of α,β-unsaturated fatty acid from the *sn*-1 substituent. Interestingly, unmodified PCs only lost the α,β-unsaturated fatty acid from the *sn*-2 substituent, not from the *sn*-1 substituent;[53] thus the terminal aldehyde on the *sn*-2 substituent of the OxPCs is likely playing some role in the formation of this product ion.

Furthermore, MS^4 of the keto-containing OxPC, KOdiAPC, yielded multiple fragmentation pathways not observed for other short-chain OxPCs; specifically, cleavages between C_2-C_3 (m/z 377) and C_3-C_4 (m/z 367) of the *sn*-2 fatty acid tail were observed. To confirm these fragmentation pathways, accurate mass measurements were performed on the hybrid LTQ FT mass spectrometer. The FTICR mass spectra obtained from MS^4 on the $[M + Na - HPO_4(CH_2)_2N(CH_3)_3]^+$ ion from KOdiAPC exhibited product ions at m/z 377.2676 (error of 2.18 ppm) and m/z 367.2856 (error of 2.10 ppm), thereby confirming the proposed molecular formulas. Although the mechanism was not confirmed, one possible rationale for the C_2-C_3 cleavage is an intramolecular retro-ene reaction involving the C_5 carbonyl group (Supporting Information Scheme S-1). This mechanism is similar to that proposed by Cheng and Gross for β-cleavage of oxofatty acids.[54] Although γ-cleavage was observed relative to the C_5 carbonyl group, the C_3-C_4 cleavage is thought to result from an intramolecular retro-ene reaction involving the C_1 carbonyl group (Supporting Information Scheme S-2), rather than 1,4-hydrogen elimination as previously reported.[54] 1,4-hydrogen elimination was considered; however, the six-membered cyclic intermediate required for 1,4-hydrogen elimination is not favorable, as the *sn*-2 tail does not contain four consecutive carbons with accessible hydrogens.

Identification of OxPCs in Spinal Cord Tissue. Following MS^n characterization of OxPC standards, $[M + Na]^+$ ions of potential OxPCs were targeted for in situ identification and MS^n imaging. Figure 5 illustrates the identification and localization of two isomeric OxPCs in spinal cord tissue. The MALDI MS spectrum obtained by averaging the mass spectra across the entire tissue section (approximately 700 scans) depicts the complex mixture of biomolecules obtained from tissue. For these in situ experiments, an important aspect of data acquisition is the selection of proper isolation windows. As described in the Experimental Section, an isolation width of 1.2 u was used for MS^2, whereas wider isolation windows were used for MS^3 and MS^4. Widening the isolation window increases the isolation efficiency, thereby maximizing the ion signal required for this type of multistage tandem MS experiments. Normally, an isolation window of this width may introduce added complexity to MS^2 spectra; however, the selectivity afforded by MS^3 and MS^4 alleviates this problem.

One potential PC oxidation product, PC(18:0/9:0 COOH), was targeted for MS^n analysis. Upon CID of the expected $[M + Na]^+$ ion (m/z 716), MS^n product ions (indicated with purple diamonds) were analogous to those predicted based on the fragmentation pathways outlined in Tables 2–4. Thus, product ions observed in the MS^2, MS^3, and MS^4 spectra allowed for in situ identification of PC(18:0/9:0 COOH). However, additional MS^2, MS^3, and MS^4 product ions (indicated with orange stars) indicated the presence of an isomeric ion at m/z 716. On the basis of these product ions, another OxPC was identified at m/z 716, $[PC(16:0/11:0\ COOH) + Na]^+$.

After collecting the MS^n spectra, extracted ion images were generated to determine the localization of the OxPCs at m/z 716 in tissue. As discussed in the Experimental Section, isolation window widths were increased for higher order MS^n spectra to enhance signal intensity; as a result, absolute intensities of MS^n product ions can be greater for higher values of n, as observed in the MS^2 and MS^3 images in Figure 5. Each image is plotted such that the color scale permits visualization of product ion localization; images generated from single-stage MS experiments are normalized to the TIC (maximum intensity values are <1.0), whereas MS^n images are plotted in absolute counts. To distinguish the gray matter from the white matter in this spinal cord section, the TIC-normalized MS image of $[PC(16:0/16:0) + Na]^+$ at m/z 756, an ion previously reported to localize in the gray matter,[43] is provided. The gray matter in this image is outlined in red; this same outline is superimposed atop the other images, demonstrating the localization of these OxPCs in the gray matter. In these images, slight variations in the spatial distribution of these product ions are observed due to scaling of each image; however in each image, the intensity of the selected ion is consistently higher in the gray matter than in the white matter. The MS^n spectra and images depicted in Figure 5 illustrate the enhanced selectivity afforded by the LIT, allowing for identification and localization of OxPCs in situ.

CONCLUSIONS

This study has established that MALDI MS^n is a powerful tool for characterizing various short-chain oxidation products of phosphatidylcholines. On the basis of the characteristic MALDI MS^n fragmentation of the $[M + H]^+$ and $[M + Na]^+$ ions of various short-chain OxPCs, valuable structural information is obtained. In MS^2, CID of the $[M + H]^+$ and $[M + Na]^+$ ions of PAzPC, PONPC, PGPC, POVPC, and KOdiAPC led to various product ions, which were analogous to those previously reported for unmodified PCs. For additional structural information, the ion corresponding to the NL of 59 from the $[M + Na]^+$ was fragmented in MS^3 and yielded multiple product ions, one of which (the NL of CO_2) was diagnostic of a terminal carboxyl group on the *sn*-2 tail. Furthermore, MS^4 of the $[M + Na]^+$ resulted in drastically different fragmentation depending on the *sn*-2 fatty acid length and type of functional groups added. An MS^4 fragmentation pathway characteristic of OxPCs containing a terminal aldehyde rather than a carboxylic acid was the NL of 254, thought to correspond to the elimination of the α,β-unsaturated *sn*-1 fatty acid substituent (16:1). Additionally, the presence of the keto group in KOdiAPC led to midchain cleavages of the *sn*-2 fatty acid moiety. While we were unable to confirm all of the product ions in Tables 2–4 by accurate mass measurements, we did obtain data to support the unexpected, midchain cleavages of KOdiAPC in MS^4.

This work also illustrates the feasibility of this MALDI MS^n methodology for the analysis and identification of individual PC oxidation products in complex mixtures including intact biological tissues. The diagnostic ions detailed in this study were utilized for targeted MALDI MS^n imaging studies to determine the distribution of OxPCs in tissue sections. Although the work presented herein was focused specifically

on short-chain OxPCs, long-chain OxPCs including hydroxylated derivatives have also been investigated and will be the subject of a subsequent manuscript. Through the development of selective methods for identifying various OxPCs and determining their in situ localization, a greater understanding of the biological and physiopathological activities of these phospholipid oxidation products may be achieved.

■ ASSOCIATED CONTENT

Supporting Information

Additional materials as described in the text. This material is available free of charge via the Internet at http://pubs.acs.org.

■ AUTHOR INFORMATION

Corresponding Author

*E-mail: ryost@ufl.edu. Phone: (352) 392-0557. Fax: (352) 392-4651.

Notes

The authors declare no competing financial interest.

■ ACKNOWLEDGMENTS

The authors would like to acknowledge Dr. Nigel Calcutt for providing the spinal cord tissue used in this work. Also, the authors thank Dr. Jodie Johnson and Ashton Bartley for insightful discussions regarding fragmentation mechanisms. This work was partially supported by the NSF MS-PIRE grant (OISE-0730072) and Eastman Chemical Company.

■ REFERENCES

(1) Markesbery, W. R.; Lovell, M. A. *Neurobiol. Aging* **1998**, *19*, 33−36.
(2) Koppaka, V.; Axelsen, P. H. *Biochemistry* **2000**, *39*, 10011−10016.
(3) Koppaka, V.; Paul, C.; Murray, I. V. J.; Axelsen, P. H. *J. Biol. Chem.* **2003**, *278*, 36277−36284.
(4) Huang, L.; Estrada, R.; Yappert, M. C.; Borchman, D. *Free Radical Biol. Med.* **2006**, *41*, 1425−1432.
(5) Berliner, J. A.; Leitinger, N.; Tsimikas, S. *J. Lipid Res.* **2009**, *50*, S207−S212.
(6) Qin, J.; Goswami, R.; Balabanov, R.; Dawson, G. *J. Neurosci. Res.* **2007**, *85*, 977−984.
(7) Baskol, G.; Demir, H.; Baskol, M.; Kilic, E.; Ates, F.; Karakukcu, C.; Ustdal, M. *Cell Biochem. Funct.* **2006**, *24*, 307−311.
(8) Yin, H.; Cox, B. E.; Liu, W.; Porter, N. A.; Morrow, J. D.; Milne, G. L. *J. Mass Spectrom.* **2009**, *44*, 672−680.
(9) Salomon, R. G.; Gu, X. *Chem. Res. Toxicol.* **2011**, *24*, 1791−1802.
(10) Sun, M. J.; Finnemann, S. C.; Febbraio, M.; Shan, L.; Annangudi, S. P.; Podrez, E. A.; Hoppe, G.; Darrow, R.; Organisciak, D. T.; Salomon, R. G.; Silverstein, R. L.; Hazen, S. L. *J. Biol. Chem.* **2006**, *281*, 4222−4230.
(11) Leitinger, N. *Curr. Opin. Lipidol.* **2003**, *14*, 421−430.
(12) Lee, S.; Birukov, K. G.; Romanoski, C. E.; Springstead, J. R.; Lusis, A. J.; Berliner, J. A. *Circ. Res.* **2012**, *111*, 778−799.
(13) Gao, D.; Ashraf, M. Z.; Kar, N. S.; Lin, D.; Sayre, L. M.; Podrez, E. A. *J. Biol. Chem.* **2010**, *285*, 4447−4454.
(14) Murphy, R. C. *Chem. Res. Toxicol.* **2001**, *14*, 463−472.
(15) Reis, A.; Spickett, C. M. *Biochim. Biophys. Acta* **2012**, *1818*, 2374−2387.
(16) Ohkawa, H.; Ohishi, N.; Yagi, K. *Anal. Biochem.* **1979**, *95*, 351−358.
(17) Schiller, J.; Süß, R.; Arnhold, J.; Fuchs, B.; Leßig, J.; Müller, M.; Petković, M.; Spalteholz, H.; Zschörnig, O.; Arnold, K. *Prog. Lipid Res.* **2004**, *43*, 449−488.
(18) Domingues, M. R. M.; Reis, A.; Domingues, P. *Chem. Phys. Lipids* **2008**, *156*, 1−12.
(19) O'Donnell, V. B. *Biochim. Biophys. Acta, Mol. Cell Biol. Lipids* **2011**, *1811*, 818−826.
(20) Bochkov, V. N.; Oskolkova, O. V.; Birukov, K. G.; Levonen, A. L.; Binder, C. J.; Stockl, J. *Antioxid. Redox Signaling* **2010**, *12*, 1009−1059.
(21) Tokumura, A.; Sumida, T.; Toujima, M.; Kogure, K.; Fukuzawa, K.; Takahashi, Y.; Yamamoto, S. *J. Lipid Res.* **2000**, *41*, 953−962.
(22) Kayganich-Harrison, K. A.; Murphy, R. C. *Anal. Biochem.* **1994**, *221*, 16−24.
(23) Watson, A. D.; Leitinger, N.; Navab, M.; Faull, K. F.; Hörkkö, S.; Witztum, J. L.; Palinski, W.; Schwenke, D.; Salomon, R. G.; Sha, W.; Subbanagounder, G.; Fogelman, A. M.; Berliner, J. A. *J. Biol. Chem.* **1997**, *272*, 13597−13607.
(24) Frey, B.; Haupt, R.; Alms, S.; Holzmann, G.; König, T.; Kern, H.; Kox, W.; Rüstow, B.; Schlame, M. *J. Lipid Res.* **2000**, *41*, 1145−1153.
(25) Nakamura, T.; Henson, P. M.; Murphy, R. C. *Anal. Biochem.* **1998**, *262*, 23−32.
(26) Hall, L. M.; Murphy, R. C. *Anal. Biochem.* **1998**, *258*, 184−194.
(27) Reis, A.; Domingues, P.; Ferrer-Correia, A. J. V.; Domingues, M. R. M. *J. Mass Spectrom.* **2004**, *39*, 1513−1522.
(28) Nakanishi, H.; Iida, Y.; Shimizu, T.; Taguchi, R. *J. Chromatogr., B: Anal. Technol. Biomed. Life Sci.* **2009**, *877*, 1366−1374.
(29) Spickett, C. M.; Rennie, N.; Winter, H.; Zambonin, L.; Landi, L.; Jerlich, A.; Schaur, R. J.; Pitt, A. R. *Biochem. J.* **2001**, *355*, 449−457.
(30) Oskolkova, O. V.; Afonyushkin, T.; Preinerstorfer, B.; Bicker, W.; von Schlieffen, E.; Hainzl, E.; Demyanets, S.; Schabbauer, G.; Lindner, W.; Tselepis, A. D.; Wojta, J.; Binder, B. R.; Bochkov, V. N. *J. Immunol.* **2010**, *185*, 7706−7712.
(31) Megli, F. A.; Russo, L. *Biochim. Biophys. Acta* **2008**, *1778*, 143−152.
(32) Domingues, M. R. M.; Simões, C.; da Costa, J. P.; Reis, A.; Domingues, P. *Biomed. Chromatogr.* **2009**, *23*, 588−601.
(33) Reis, A.; Domingues, P.; Ferrer-Correia, A. J. V.; Domingues, M. R. M. *Rapid Commun. Mass Spectrom.* **2004**, *18*, 2849−2858.
(34) Reis, A.; Domingues, M. R. M.; Amado, F. M. L.; Ferrer-Correia, A. J. V.; Domingues, P. *Biomed. Chromatogr.* **2005**, *19*, 129−137.
(35) Stübiger, G.; Belgacem, O. *Anal. Chem.* **2007**, *79*, 3206−3213.
(36) van den Brink, O. F.; Boon, J. J.; O'Connor, P. B.; Duursma, M. C.; Heeren, R. M. A. *J. Mass Spectrom.* **2001**, *36*, 479−492.
(37) Bischoff, A.; Eibisch, M.; Fuchs, B.; Suss, R.; Schurenberg, M.; Suckau, D.; Schiller, J. *Acta Chromatogr.* **2011**, *23*, 365−375.
(38) Fuchs, B.; Bresler, K.; Schiller, J. *Chem. Phys. Lipids* **2011**, *164*, 782−795.
(39) Stubiger, G.; Belgacem, O.; Rehulka, P.; Bicker, W.; Binder, B. R.; Bochkov, V. *Anal. Chem.* **2010**, *82*, 5502−5510.
(40) Garrett, T. J.; Prieto-Conaway, M. C.; Kovtoun, V.; Bui, H.; Izgarian, N.; Stafford, G.; Yost, R. A. *Int. J. Mass Spectrom.* **2007**, *260*, 166−176.
(41) Menger, R. F.; Stutts, W. L.; Anbukumar, D. S.; Bowden, J. A.; Ford, D. A.; Yost, R. A. *Anal. Chem.* **2011**, *84*, 1117−1125.
(42) Garrett, T. J.; Yost, R. A. In *Mass Spectrometry Imaging: Principles and Protocols*; Rubakhin, S. S., Sweedler, J. V., Eds.; Humana Press: New York, 2010; Vol. *656*, pp 209−230.
(43) Landgraf, R. R.; Prieto-Conaway, M. C.; Garrett, T. J.; Stacpoole, P. W.; Yost, R. A. *Anal. Chem.* **2009**, *81*, 8488−8495.
(44) Sparvero, L. J.; Amoscato, A. A.; Kochanek, P. M.; Pitt, B. R.; Kagan, V. E.; Bayır, H. *J. Neurochem.* **2010**, *115*, 1322−1336.
(45) Karas, M.; Hillenkamp, F. *Anal. Chem.* **1988**, *60*, 2299−2301.
(46) Schwartz, S. A.; Reyzer, M. L.; Caprioli, R. M. *J. Mass Spectrom.* **2003**, *38*, 699−708.
(47) Garrett, T. J.; Yost, R. A. *Anal. Chem.* **2006**, *78*, 2465−2469.
(48) Domingues, P.; Domingues, M. R. M.; Amado, F. M. L.; Ferrer-Correia, A. J. *Rapid Commun. Mass Spectrom.* **2001**, *15*, 799−804.
(49) Pulfer, M.; Murphy, R. C. *Mass Spectrom. Rev.* **2003**, *22*, 332−364.
(50) Hsu, F.-F.; Turk, J. *J. Am. Soc. Mass Spectrom.* **2003**, *14*, 352−363.
(51) Han, X.; Gross, R. W. *J. Am. Soc. Mass Spectrom.* **1995**, *6*, 1202−1210.

(52) Hsu, F.-F.; Turk, J. *J. Am. Soc. Mass Spectrom.* **2010**, *21*, 657–669.
(53) Hsu, F.-F.; Turk, J. *J. Chromatogr., B: Anal. Technol. Biomed. Life Sci.* **2009**, *877*, 2673–2695.
(54) Cheng, C.; Gross, M. *J. Am. Soc. Mass Spectrom.* **1998**, *9*, 620–627.